IEEE Access
Multidisciplinary ⋮ Rapid Review ⋮ Open Access Journal

Received 25 July 2024, accepted 29 August 2024, date of publication 3 September 2024, date of current version 12 September 2024.

Digital Object Identifier 10.1109/ACCESS.2024.3453905

RESEARCH ARTICLE

Pattern Diversity Antenna for 5G-NR Application Based on Closely-Spaced Semi-Circular Slots

YOUNGJE SUNG
Department of Electronic Engineering, Kyonggi University, Suwon-si 16227, South Korea
e-mail: yjsung@kgu.ac.kr

This work was supported in part by the Technology Innovation Program under Grant 20017411; in part by the Ministry of Trade, Industry and Energy (MOTIE), South Korea, through the Development of Gen.10 OLED Evaporation Core Modules for TV; and in part by the National Research Foundation of Korea (NRF) Grant funded by Korean Government (MSIT) under Grant 2022R1A4A5028239.

ABSTRACT In this study, a dual-feed polarization diversity antenna with a broadside or conical radiation pattern is proposed for fifth-generation (5G)-NR applications. The antenna's design incorporates a radiator created using a circular slot, segmented into two semicircular slots by a protruding stub. By adjusting the phase difference applied to these two semi-circular slots, different radiation patterns within the same frequency band can be achieved. A modified 180° rat-race coupler served as the feed structure. By analyzing current distribution and E-field distribution, the phase difference formed in the two semi-circular slots according to the input terminal is confirmed. The measurement results showed that the proposed antenna exhibited polarization diversity characteristics across a bandwidth of 12.7% (3.24∼3.7GHz), with isolation exceeding 25 dB between the two input terminals. In this case, the measured gains are 5.2 dBi for Port 1 and 3.5 dBi for Port 2.

INDEX TERMS Pattern diversity antenna, slot antenna, fifth-generation (5G), hybrid coupler, wideband antenna.

I. INTRODUCTION

As wireless mobile communication develops rapidly, data traffic increases exponentially, necessitating additional bandwidths to accommodate various services. Multiple input multiple output (MIMO) wireless transmission technology can enhance wireless transmission capacity without requiring additional spectrum resources [1]. Using multiple antennas allows for the reception of signals from different paths simultaneously, thereby alleviating signal fading [2], [3]. Consequently, the quality and reliability of wireless links can be improved. Antenna diversity technology lies at the core of MIMO systems, especially in the case of 5G-NR. However, an increase in the number of antennas increases the volume and price of the system [4].

A pattern diversity antenna reduces blind spots by implementing radiation patterns with different null positions simultaneously, thereby avoiding noisy environments and increasing environmental adaptability. In addition, by appropriately adjusting the direction of the signal to the target, the energy consumption of a system can be minimized, and coverage can be expanded by redirecting the main beam's direction [5], [6].

Pattern diversity antennas can be classified into types. First, two identical antennas with directional radiation patterns are used, and their radiation pattern's direction are independently adjusted by solely modifying the positions of the antennas using the antenna shape, without redesigning [7], [8], [9]. To obtain isolation between antennas, either an appropriate separation distance is necessary or a decoupling structure is applied between the antennas. In [10], massive MIMO technology was applied by increasing the number of directional antennas to four or six. However, due to the necessity of a separation distance in this setup involving two antennas, the overall size of the antenna became inevitably large.

Second, two antennas with different shapes are used, resulting in distinct radiation patterns (example, broadside and conical radiation patterns). This structure avoids increasing the overall size through various methods, such as

The associate editor coordinating the review of this manuscript and approving it for publication was Debabrata K. Karmokar.

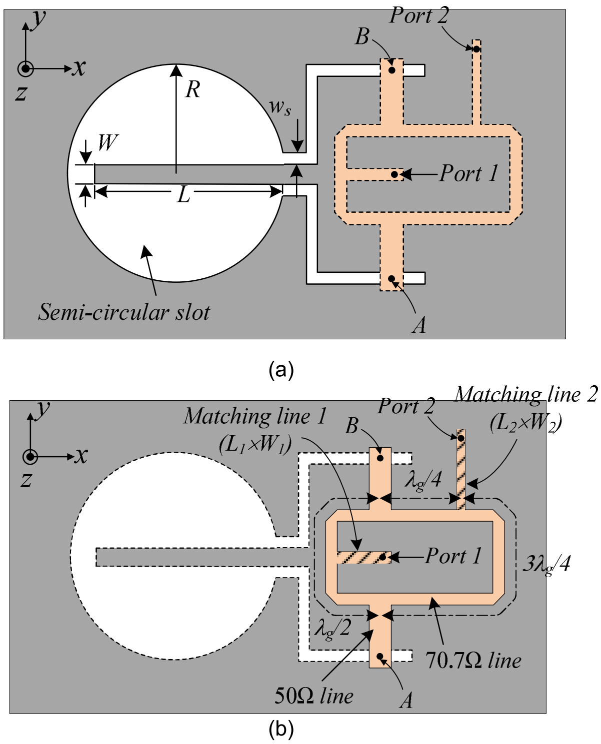

FIGURE 1. **Pattern diversity antenna featuring a circular slot with a protruded stub. (top layer: gray, bottom layer: orange). (a) top view. (b) bottom view.**

inserting a ring inside a ring resonator [11], combining monopole and dipole antennas [12], placing a folded monopole under a top-loaded antenna [13], or placing circular patch inside a cup-shaped patch. However, good isolation characteristics need to be achieved due to the extremely close proximity of the two antennas. A DM/CM antenna can achieve high isolation and complementary patterns, even when the radiators of the DM and CM antennas overlap [14].

Antennas combining two resonators increase in height or size, making them unsuitable for practical applications. Accordingly, many pattern diversity antennas with a single resonator have been proposed recently [15], [16], [17], [18], [19]. These structures were designed based on the variation in the mode formed within the resonator depending on the feed point. In other words, this technique enables pattern diversity through the design of the feed structure rather than the radiator itself.

A pattern diverse antenna utilizing reconfigurable technology has also been proposed. Unlike other designs, this structure does not prioritize isolation during its design phase. However, it comes with disadvantages such as distortion of the radiation pattern caused by the bias line, performance degradation, and increased DC power consumption [20], [21].

In this paper, a pattern diversity antenna for 5G-NR applications is proposed. The remarkable features of the proposed structure are as follows. First, pattern diversity is implemented based on adjacent semi-circular slots by dividing one circular slot in half. Second, the operating bandwidth of the

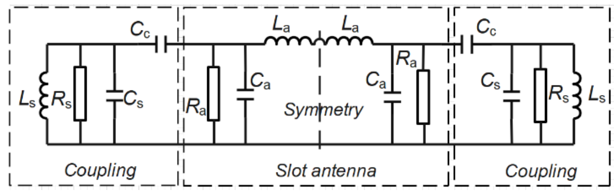

FIGURE 2. **Equivalent circuit model of the slot antenna and the coupling between antenna and feed without considering the hybrid coupler.**

pattern diversity antenna is increased by using a modified hybrid coupler. Third, pattern diversity is implemented by applying a meander line with inductance at the end of the protruded stub.

II. GEOMETRY

Fig. 1 shows the proposed antenna with pattern diversity, exhibiting both broadside and conical radiation patterns. This antenna comprised a circular slot antenna with radius R, a protruded stub with length L and width W, and modified 180° hybrid coupler. The slot antenna and GND were implemented on the rear side of the substrate, corresponding to the gray area in Fig. 1. Meanwhile, the 180° hybrid coupler was implemented on the bottom side of the substrate, corresponding to the orange area. The circular slot antenna was divided into two semicircular slots by a protruded stub intersecting the slot, and RF power was coupled from the hybrid coupler to each semicircular slot antenna at points A and B. The substrate has a dielectric constant of 2.2 and a thickness of 62 mils.

Ports 1 and 2, serving as the input ports of the 180° hybrid coupler, use a probe feed. A matching line was introduced between these ports and the coupler to enhance the operating bandwidth. Notably, when RF power was fed into port 1, the phases of the signals reaching points A and B, representing the lower and upper lines, respectively, were identical. Consequently, signals with matching phases were applied to the two semicircular slots. Simulation is carried out using HFSS.

Fig. 2 shows the equivalent circuit model of two half circular slot antenna pair. In the radiating element circuit model, C_a, L_a, and R_a represent the capacitance, inductance, and radiation resistance of the half circular slot antenna, respectively. In the coupling circuit model, C_c represents the coupling effect between the microstrip and the slot, C_s, L_s, and R_s represent the capacitive effect, inductive effect, and loss in the substrate, respectively. When the circuit is excited by CM or DM signals, the center symmetry plane can be equivalent to PMC or PEC, respectively. Therefore, in the equivalent circuit model, the resonant frequencies of CM and DM are same as follow.

$$f_{DM} = f_{CM} = \frac{1}{2\pi\sqrt{L_a C_a}} \tag{1}$$

To set the operating frequency for 5G-NR services, three types of antennas are studied, as shown in Fig. 3 (a). The radius of the circular slot is all set to 23 mm. The resonant

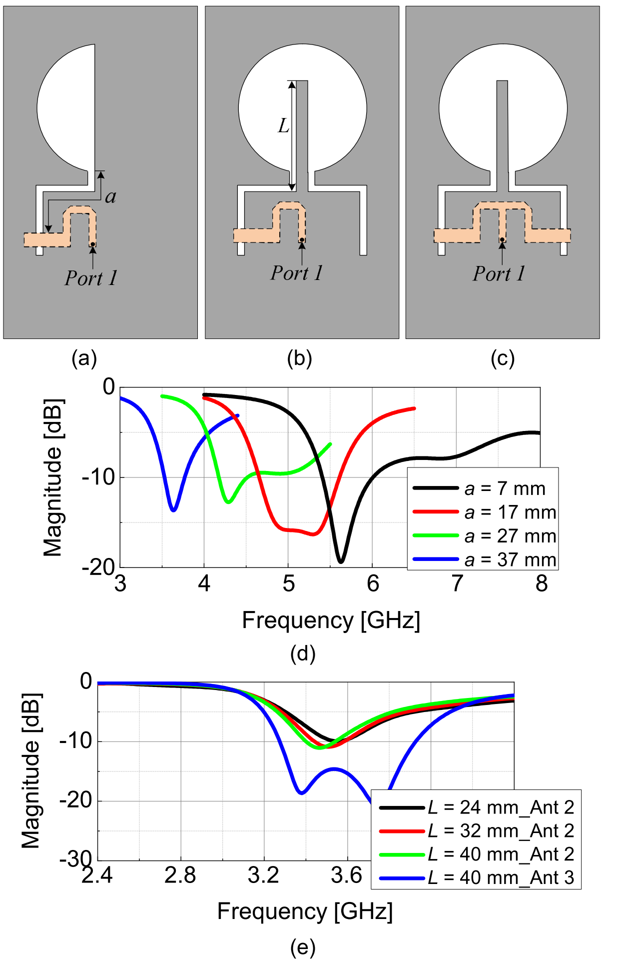

FIGURE 3. **Various types of single feed slot antennas. (a) Ant. 1. (b) Ant. 2. (c) Ant. 3. (d) Performance of Ant. 1 according to changes in length *a*. (e) Performance of Ants. 2 and 3 according to changes in length *L*.**

frequency of circular patch antenna for the TM_{mn} mode is as follows.

$$f_{mn} = \frac{\chi_{mn}c}{2\pi R\sqrt{\varepsilon_r}} \quad (2)$$

where χ_{mn} is the mth zero of $J_n'(ka)$ and c is the velocity of light in free space. Since circular slots and circular patches can be interpreted identically based on Babinet's Principle, the above equation can also be applied to the circular slot structure. In this paper, TM_{11} mode is the dominant mode, so it has $\chi_{11} = 1.84118$ [22].

Ant 1. is an antenna that has only one semi-circular slot. In here, a is the distance from the coupling point between the microstrip line and slotline to the antenna. As shown in Fig. 3 (d), as a increases, the resonant frequency of the antenna decreases. In other words, the operating frequency of the antenna is affected by the length of the mirostrip-to-slotline transition.

Ant. 2 consists of two semi-circular slots and a simple microstrip line without a hybrid coupler. As shown in Fig. 3 (e), there is little difference in the resonant frequency of the antenna as the length of L changes. At this time, a is fixed at 37mm. Unlike Ant. 2, a feed structure with a power divider is used in Ant. 3. Other parameters are the same. As is well known, the feed structure with a power divider has been widely used because it has the advantage of widening the bandwidth [23], [24].

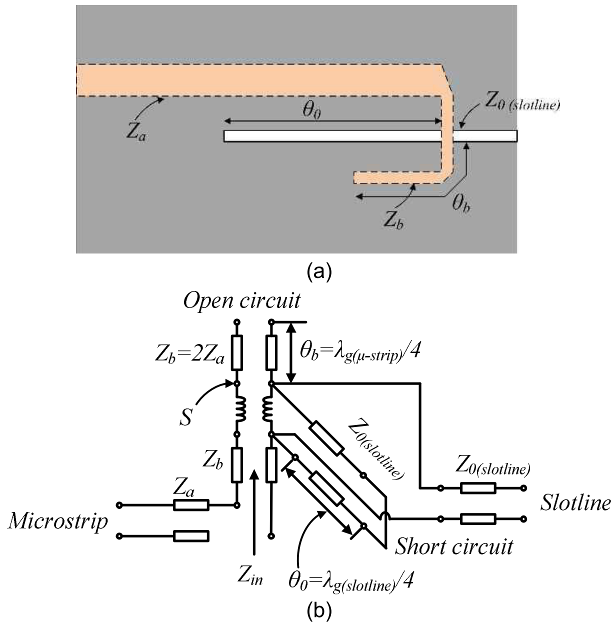

FIGURE 4. **Microstrip to slotline transition (a) Configuration. (b) Equivalent circuit.**

In this work, the folded structure consisting of open/short circuits with one $\lambda_g/4$ length is employed for impedance matching between the 100Ω microstrip line and the characteristic impedance of the slotline which represents $Z_{0(slotline)}$. Because the point 'S' in Fig. 4 (b) is virtually shorted by the open-circuited microstrip line with one $\lambda_g/4$ length, the matching between a microstrip line mode and a slotline mode can be achieved. And the impedance matching can be easily obtained by removing the effect of the open/short circuits in Z_{in}. The input impedance Z_{in} shown in Fig. 4 (b) can be expressed by [25]

$$Z_{in} = -jZ_b cot\ \theta_b + \frac{jZ_{0(slotline)}Z_{0(slotline)}tan\ \theta_{ab}}{Z_{0(slotline)}+jZ_{0(slotline)}tan\ \theta_{ab}} \quad (3)$$

where $Z_{0(slotline)}$ is the characteristic impedance of the slotline, and Z_b and θ_b are the characteristic impedance and the electrical length of the open-circuited microstrip line, respectively. $Z_{0(slotline)}$ is the characteristic impedance slotline. θ_{ab} is the electrical length of the short-circuited slotline. Thus, the input impedance in Eq. (3) can be reduced as follows:

$$Z_{in} = Z_{0(slotline)} \quad (4)$$

A similar antenna structure was also proposed by the author in [25]. However, both antennas have the following structural differences. In [25], to obtain good circular polarization characteristics, the length of the protruded stub was set to

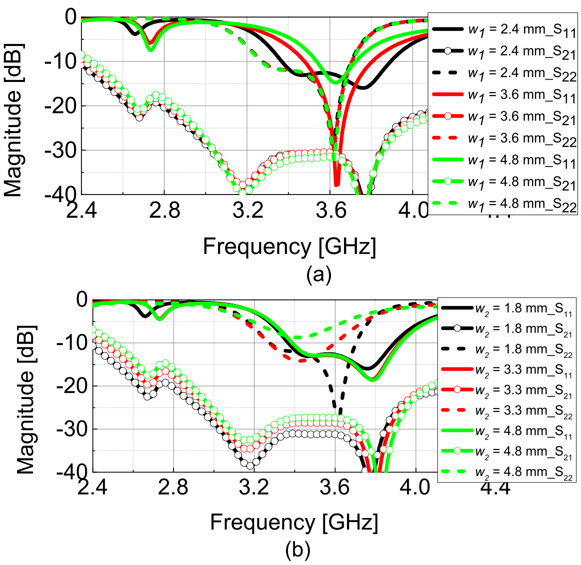

FIGURE 5. Simulation results illustrating antenna performance with alterations in line width. (a) Variation in W_1, and (b) Variation in W_2.

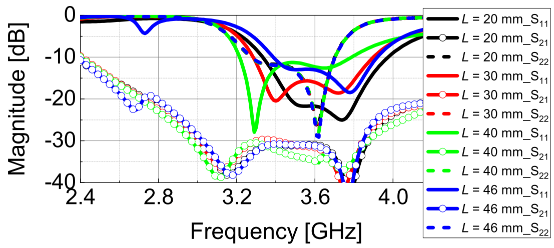

FIGURE 6. Simulation results according to the length L of the protruded stub.

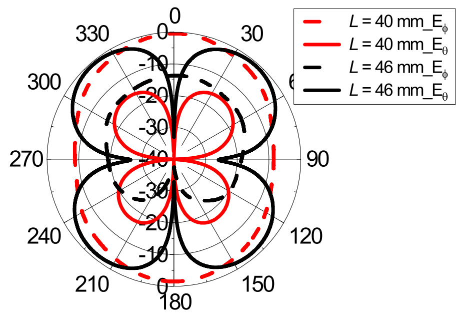

FIGURE 7. Comparison of ideal radiation patterns in the xz-plane.

be smaller than $2R$, which is the diameter of the circular slot, ensuring that the slot was not perfectly divided into two semicircular slots. As discussed subsequently, employing the same structure in this study did not yield a conical radiation pattern when RF power was applied to port 1, as aforementioned. Consequently, a chip inductor or meander line is connected between the end of the slot and protruded stub. In terms of performance, the two structures exhibit the following differences: In [25], dual-feed polarization diversity characteristics were obtained by implementing two circular polarization characteristics. In contrast, this study achieved dual-feed radiation pattern-diversity characteristics.

III. PATTERN DIVERSITY ANTENNA

If the impedances of ports 1 and 2 were set to 50Ω, similar to a conventional 180° hybrid coupler, a single resonance is formed in S_{11} and S_{22}. Consequently, the operating bandwidth of the antenna with polarization diversity was restricted to less than 2%. This limitation inevitably narrows the application field. To broaden the bandwidth, the impedance of the input stage was adjusted, corresponding to W_1 of matching line 1 and W_2 of matching line 2, as shown in Fig. 1. Fig. 5 shows the simulation results of the antenna performance as linewidths W_1 and W_2 vary. Apart from W_1 and W_2, the remaining parameters were set as follows: $R = 23$ *mm*, $L = 46$ *mm*, $W = 4.3$ *mm*, $w_s = 0.7$ *mm*, $L_1 = 12$ *mm*, and $L_2 = 18$ *mm*.

The line width of 4.8 *mm* corresponds to 50Ω of the substrate used. The simulation results show that, as the width increases, the impedance of the line decreases. As it approaches 50Ω, the number of resonances reduces from two to one, and the matching deteriorates. In addition, when W_1 is changed, only the frequency response of S_{11} is affected, and when W_2 is changed, only the frequency response of S_{22}. is affected. This phenomenon occurred because the isolation characteristics between ports 1 and 2 were good. In addition, in the case of port 2, when w_2 is selected as 1.8 *mm* instead of 4.8 *mm*, the S_{21} characteristic is also improved by approximately 5 dB.

Fig. 6 shows the simulation results of the antenna with the length L of the protruded stub blocking the circular slot. The remaining parameters were as aforementioned. The simulation results show that the length L of the protruding stub affects the reflection coefficient at port 1, while the reflection coefficient and isolation at port 2 remain unchanged.

The core technology of pattern diversity antennas lies in implementing different patterns at the same frequency. Thus, the common band between the operating frequency bands in ports 1 and 2 can be defined as the operating frequency band of the pattern diversity antenna. L emerges as a potential parameter for optimizing the common bands of ports 1 and 2 because it does not affect the frequency response of S_{22}. but does influences that of S_{11}. If L exceeds 30 mm, the operating frequency band of S_{11} includes that of S_{22}, resulting in the proposed antenna having the maximum operating bandwidth. Therefore, a value of 40*mm* is selected for L, considering the margins at the lower and upper parts of the common bandwidth. Because the radius R of the circular slot is 23*mm*, the semicircular slot is completely separated by the protruding stub when L is 46 mm. At this point, the frequency response of S_{11} increased, and the common bands of S_{11} and S_{22}. are significantly reduced.

When L is 40*mm*, the two semicircular slots are partially connected, and when L is 46*mm*, the semicircular slots are completely separated into two using a protruding stub.

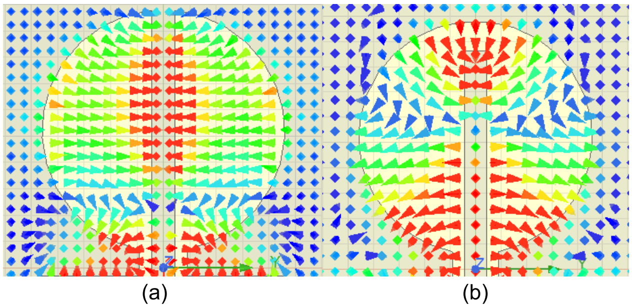

FIGURE 8. **E-field distribution for port 1 excitation at (a)** $L = 46$ **mm, and (b)** $L = 40$ **mm.**

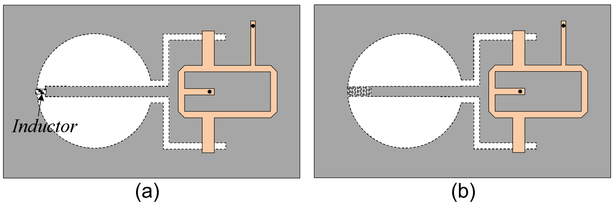

FIGURE 9. **Antenna with inductor applied to the slot end utilizing (a) chip inductor, and (b) meander line.**

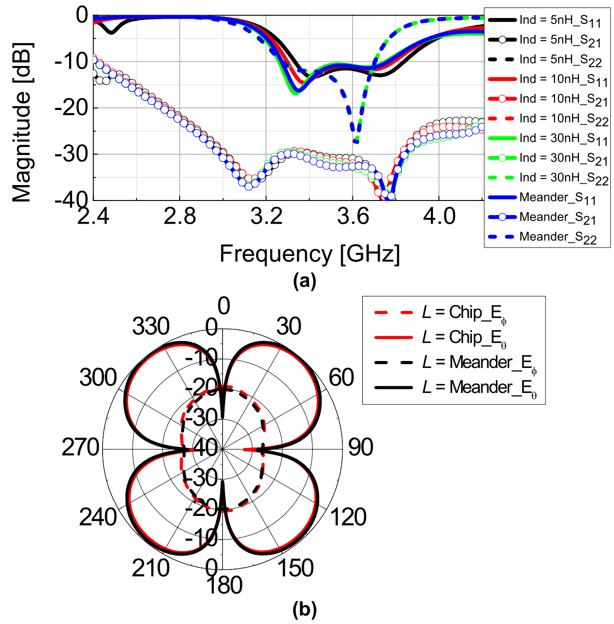

FIGURE 10. **Simulation results according to chip inductor value (a) Frequency response, and (b) radiation pattern.**

Figs.7 (a) and (b) compare the *yz*-plane radiation patterns for both cases when power is applied to ports 1 and 2, respectively. When power is applied to port 2, the same broadside radiation pattern is formed whether the protruding stub is connected or disconnected from the end of the slot. When power is applied to port 1, the radiation pattern is varied depending on L. At an L of 46*mm*, an observed conical radiation pattern contrasts with one that closely resembles the broadside radiation pattern at 40*mm*. However, this study indicates that the radiation pattern at port 2 becomes inappropriate when L is 40*mm*, as it exhibits different radiation patterns within the same frequency band.

Fig. 8 shows the E-field distribution within the slot for L values of 46*mm* and 40*mm*. When L is 46*mm*, the electric field is formed horizontally within the slot, exhibiting opposing directions on the left and right sides due to the presence of the stub. Accordingly, a conical radiation pattern is generated when L is 46*mm*. When L is 40*mm*, the electric field is formed vertically within the slot. At this point, the maximum E-field intensity occurs at the top and bottom of the slot, with a phase difference approximately 180° between them. Therefore, a broadside radiation pattern is generated.

As shown in Figs. 6–8, the following conclusions can be drawn: From the perspective of the frequency response (S_{11} and S_{22}.), the circular slots are not entirely separated by the stub. However, from the perspective of the radiation pattern, completely separation of the circular slot by the stub is preferable. To determine the advantages of using both structures simultaneously, we propose a configuration wherein the end of the stub connects to an inductor, as shown in Fig. 9.

The inductor depicted in Fig. 9 serves two functions. First, it divides the left and right sides of the circular slot, facilitating the intended formation of a conical radiation pattern when RF power is incident on port 1. Second, from an RF perspective, the inductor electrically separates the circular slot, enabling the attainment of the desired frequency response of S_{11}.

Fig. 10 shows the antenna performance as the value of the inductor applied to the stub changes. The simulation results show that with an increase in the inductor value, the frequency response of S_{11} gradually decreases. Additionally, slight changes in S_{22} and S_{21} are observed. Notably, when the inductor value reaches 15 nH, the lower edge of the S_{11} bandwidth coincides with that of the S_{22} bandwidth, suggesting that the operating bandwidth of the polarization-diversity antenna does not extend further when the inductor value exceeds 15 *nH*. Due to the discontinuous distribution of lumped element, achieving the desired value becomes challenging, thus limiting the usable frequency range. Therefore, in this study, the meander structure, characterized by its distributed element, is explored. The width and spacing of the meander line were both set to 0.2 *mm*. The relationships between the lumped components and the distributed microstrip parameters are presented in [27]

$$L\,(\text{nH}) = 0.2l\left[\text{In}\left(\frac{l}{W+l}\right) + 1.193 + \frac{W+l}{3l}\right] \times \left(0.57 - 0.145\text{In}\frac{W}{l}\right) \quad (5)$$

As shown in Fig. 10 (b), when port 1 was used as an input port, the radiation pattern confirms to the expected conical shape.

In the conventional 180° hybrid coupler, the distances from port 2 to the two different output ports were set to

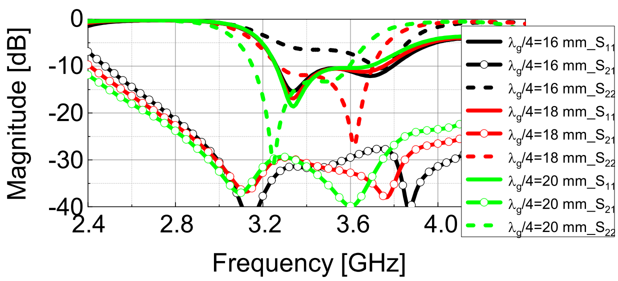

FIGURE 11. Simulation results of antenna performance according to the location of Port 2.

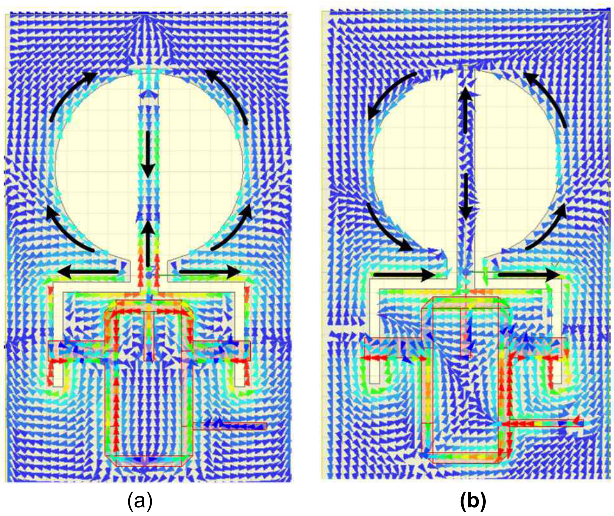

FIGURE 12. Current distribution when (a) port 1 is excited, and (b) port 2 is excited.

$3\lambda_g/4$ and $\lambda_g/4$, where λ_g is the wavelength at the design frequency. In other words, the distances from port 2 to the output terminals at points A and B were $3\lambda_g/4$ and $\lambda_g/4$, respectively. In this study, the position of port 2 was adjusted such that the distance from port 2 to the output port at point A was three times that from port 2 to the output port at point B. This adjustment ensures a phase difference of 180° between port 2 and the two output ports. Meanwhile, the distance from port 1 to the two output ports was fixed at 14*mm*.

Fig. 11 shows the distance between port 2 and point *B*. The frequency responses of S_{21} and S_{22} are affected by the variation in distance from port 2 to the output port, resulting in a slight change in S_{11}. The simulation results show that as the distance from port 2 to the output port increases, the frequency response of S_{22} decreases. As shown in Figs. 3, 7, and 8, the frequency response of S_{11} is influenced by the length of the stub or the value of the inductor applied to its end, whereas the frequency response of S_{22} can be adjusted by varying the distance from port 2 to the output terminal. Consequently, the bandwidth of the pattern-diversity antenna can be optimized by expanding the overlapping range of the bandwidths of S_{11} and S_{22}.

Fig. 12 (a) shows that when power is applied to port 1, the phases of the two output ports are equal. The current passing

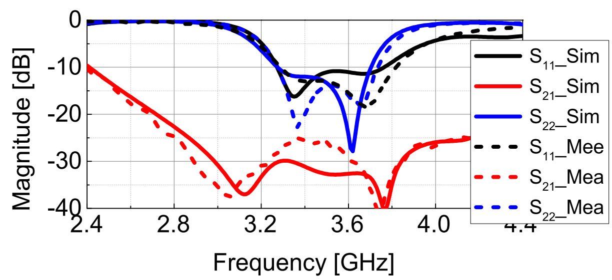

FIGURE 13. Simulated and measured frequency response of the proposed antenna.

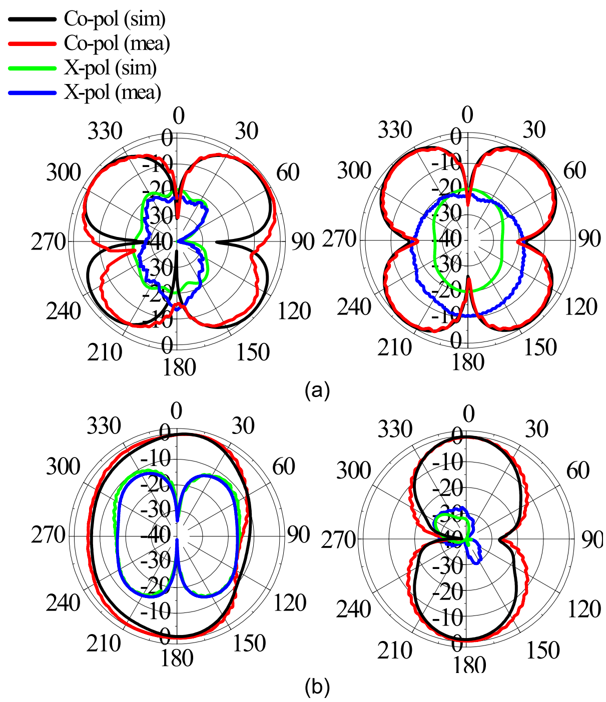

FIGURE 14. Simulated and measured radiation pattern in the *xz*- and *yz*-planes. (a) port 1. (b) port 2.

through the narrow slit is formed in opposite directions on the left and right sides. Consequently, a current distribution is established where the left and right semicircular slot antennas exhibit a phase difference of 180°, thereby forming an even mode. Due to the opposing directions of semi-circular slot antennas, this current distribution generates a conical radiation pattern. Considering the current distribution formed on the center strip line, currents flowing from top to bottom and from bottom to top coexist, creating an offset effect. This phenomenon explains the excellent isolation characteristics of the left and right antennas.

In Fig. 12 (b), the scenario is depicted where RF power is applied from port 2, and the two output ports of a typical 180° hybrid coupler are utilized to achieve a 180° phase difference. In this configuration, the current coupled to the narrow slit is formed in the same direction, yielding an odd mode. Due to the opposing orientations of the semicircular slot antennas, the current distribution produces a broad-side radiation pattern. When considering the current distribution formed in the

TABLE 1. Comparison with previous polarization diversity antennas.

Ref.	Fre. [GHz]	BW [%]	Isolation	# of resonator	Pattern	Gain	Size
[7]	1.8	13.8	20	2	B/B	1.39	$0.72\lambda_0 \times 0.72\lambda_0$
[8]	3.5	4.5	20	2	B/B	2.1	$0.7\lambda_0 \times 0.54\lambda_0$
[9]	2.4	4.5	15	1	B/B	4.8	$0.64\lambda_0 \times 0.64\lambda_0$
[11]	2.48	4.1	30	2	B/C	2.8/-2.8	$0.76\lambda_g \times 0.74\lambda_g$
[12]	3.5	14.1	22	1	B/C	7.48/3.15	$0.51\lambda_0 \times 0.24\lambda_0 \times 0.005\lambda_0$
[13]	2.2	48.3	30	2	B/C	11/7.2	$1.1\lambda_0 \times 1.1\lambda_0 \times 0.11\lambda_0$
[14]	3.5	5.5	24	2	B/C	6/5.71	$0.33\lambda_0 \times 0.058\lambda_0 \times 0.019\lambda_0$
[18]	2.4	44	20	2	B/C	9.9/8.4	$2r=2\lambda_0$ $h=0.2\lambda_0$
[17]	2.5	28.5	23	2	B/C	9.9/7	$2r=2.97\lambda_0$ $h=0.066\lambda_0$
[19]	5.2	2.5	27	1	B/C	4.5/4.8	$2r=0.62\lambda_0$
This work	3.5	12.7	20	1	B/C	5.2/3.5	$1.1\lambda_0 \times 1.1\lambda_0$

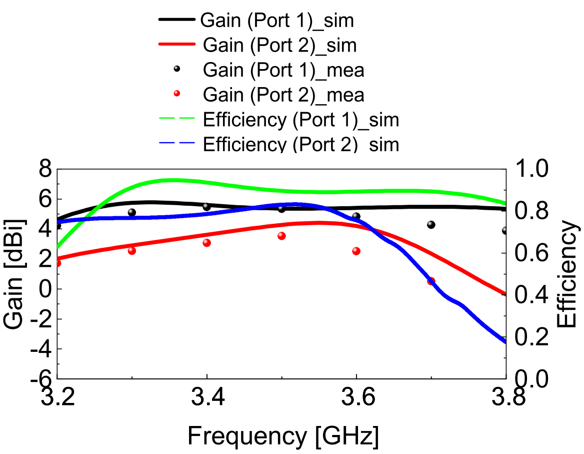

FIGURE 15. Simulated and measured gain and efficiency.

center stripline, the overall currents flow from top to bottom and from bottom to top, leading to a canceling effect.

IV. SIMULATED AND MEASURED RESULTS

A prototype of the proposed antenna was fabricated and tested. Fig. 13 shows the simulated and measured S-parameters of the proposed antenna. The measured 10 dB bandwidths for port 1 and port 2 are 500 MHz (3.24–3.74 GHz) and 580 MHz (3.24–3.82 GHz), respectively. The overlapping bandwidth was 445 MHz (3.29–3.735 GHz), or 12.7%, corresponding to 3.5 GHz. The port isolation exceeds 25 dB across the entire bandwidth, and the measurements align closely with the simulation results. There are some errors in the peak positions for S_{11} and S_{22}. Any observed differences between the simulated and measured results can be attributed to fabrication tolerances.

Fig. 14 depicts the simulated and measured radiation patterns corresponding to the excitation of each port in the xz and yz-planes. Each port was measured individually with the other terminated using a Ω50 load. The radiation patterns of the two beams were complementary. Any difference between the simulated and measured radiation patterns can be attributed to fabrication tolerances. The measured gain in ports 1 and 2 are 5.23 and 3.51 dBi, respectively. Fig. 15 shows a photograph of the fabricated antenna. As presented in Table 1, the performance of previous polarization diversity antennas is compared with that of the proposed antenna.

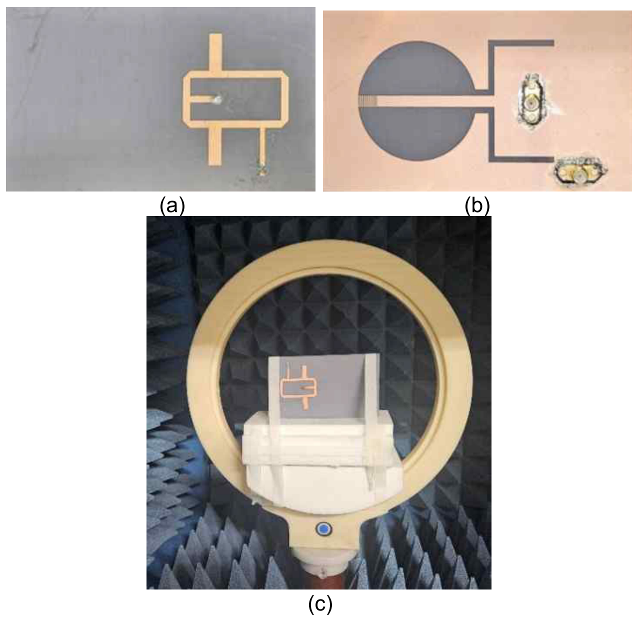

FIGURE 16. Photograph of the fabricated antenna. (a) top (b) bottom. (c) the proposed antenna under measurement.

V. CONCLUSION

In this study, a dual-feed pattern-diversity antenna is proposed. The proposed structure exhibited three remarkable features. First, despite the close proximity of the two semicircular antennas, the isolation characteristics remained strong, surpassing 25 dB within the operating band. Second, the operating bandwidth was enhanced by incorporating a matching section at the input terminal. Third, a meandering line with an inductance component was introduced at the end of the stub between the two semicircles to preserve wide bandwidth characteristics and prevent distortion of the radiation pattern. The proposed work is a good candidate for 5G-NR applications.

REFERENCES

[1] A. Yang, Y. Jing, C. Xing, Z. Fei, and J. Kuang, "Performance analysis and location optimization for massive MIMO systems with circularly distributed antennas," *IEEE Trans. Wireless Commun.*, vol. 14, no. 10, pp. 5659–5671, Oct. 2015.

[2] Y. Zhang, J. Ge, and E. Serpedin, "Performance analysis of nonorthogonal multiple access for downlink networks with antenna selection over Nakagami-*m* fading channels," *IEEE Trans. Veh. Technol.*, vol. 66, no. 11, pp. 10590–10594, Nov. 2017.

[3] D. Kwon, H. Ko, S. Hong, K. Yoon, B. Cho, and K. S. Kim, "Elevation estimation algorithm for low-altitude targets in multipath environment," *J. Electromagn. Eng. Sci.*, vol. 24, no. 4, pp. 341–349, Jul. 2024.

[4] R. S. Kshetrimayum, M. Mishra, S. Aïssa, S. K. Koul, and M. S. Sharawi, "Diversity order and measure of MIMO antennas in single-user, multiuser, and massive MIMO wireless communications," *IEEE Antennas Wireless Propag. Lett.*, vol. 22, pp. 19–23, 2023.

[5] M. Borhani-Kakhki, A. Dadgarpour, M. A. Antoniades, A. R. Sebak, and T. A. Denidni, "Magnetoelectric dipole antennas loaded with meta-lens for 5G MIMO pattern diversity applications," *IEEE Trans. Antennas Propag.*, vol. 70, no. 8, pp. 7112–7117, Aug. 2022.

[6] Z. Chen, J. Tian, H. Liu, J. Yu, and X. Chen, "Novel pattern-diverse millimeter-wave antenna with broadband, high-gain, enhanced-coverage for energy-efficient unmanned aerial vehicle," *IEEE Trans. Veh. Technol.*, vol. 70, no. 5, pp. 4081–4087, May 2021.

[7] Y. Sung, "A dual orthogonal fed monopole antenna for circular polarization diversity," *J. Electromagn. Eng. Sci.*, vol. 22, no. 3, pp. 283–290, May 2022.

[8] C. F. Ding, X. Y. Zhang, C.-D. Xue, and C.-Y.-D. Sim, "Novel pattern-diversity-based decoupling method and its application to multielement MIMO antenna," *IEEE Trans. Antennas Propag.*, vol. 66, no. 10, pp. 4976–4985, Oct. 2018.

[9] Y. S. Kim and D.-H. Cho, "Design of four-port integrated monopole antenna using refraction effect of dielectric medium for pattern gain enhancement," *IEEE Antennas Wireless Propag. Lett.*, vol. 19, pp. 621–625, 2020.

[10] Y. Kabiri, A. L. Borja, J. R. Kelly, and P. Xiao, "A technique for MIMO antenna design with flexible element number and pattern diversity," *IEEE Access*, vol. 7, pp. 86157–86167, 2019.

[11] S. Maddio, "A circularly polarized switched beam antenna with pattern diversity for WiFi applications," *IEEE Antennas Wireless Propag. Lett.*, vol. 16, pp. 125–128, 2017.

[12] Z. Wang, Y. Ning, and Y. Dong, "Compact shared aperture quasi-yagi antenna with pattern diversity for 5G-NR applications," *IEEE Trans. Antennas Propag.*, vol. 69, no. 7, pp. 4178–4183, Jul. 2021.

[13] Y. Zheng, G. A. E. Vandenbosch, and S. Yan, "Low-profile broadband antenna with pattern diversity," *IEEE Antennas Wireless Propag. Lett.*, vol. 19, pp. 1231–1235, 2020.

[14] H. Xu, S. S. Gao, H. Zhou, H. Wang, and Y. Cheng, "A highly integrated MIMO antenna unit: Differential/common mode design," *IEEE Trans. Antennas Propag.*, vol. 67, no. 11, pp. 6724–6734, Nov. 2019.

[15] Y. Zheng and S. Yan, "A low-profile half-mode annular microstrip antenna with pattern diversity," *IEEE Antennas Wireless Propag. Lett.*, vol. 19, pp. 1739–1743, 2020.

[16] N. Yang and K. W. Leung, "Compact cylindrical pattern-diversity dielectric resonator antenna," *IEEE Antennas Wireless Propag. Lett.*, vol. 19, pp. 19–23, 2020.

[17] S. Tang, N. Liu, J. Chen, X. Wang, G. Fu, and L. Zhu, "Low-profile wideband patch antenna with pattern diversity using custom-designed feeding schemes," *Int. J. RF Microw. Comput.-Aided Eng.*, vol. 31, no. 12, Dec. 2021.

[18] N. Yang, K. W. Leung, and N. Wu, "Pattern-diversity cylindrical dielectric resonator antenna using fundamental modes of different mode families," *IEEE Trans. Antennas Propag.*, vol. 67, no. 11, pp. 6778–6788, Nov. 2019.

[19] C. Deng, Z. Zhao, and W. Yu, "Characteristic mode analysis of circular microstrip patch antenna and its application to pattern diversity design," *IEEE Access*, vol. 10, pp. 2399–2407, 2022.

[20] K. Saurav, N. K. Mallat, and Y. M. M. Antar, "A three-port polarization and pattern diversity ring antenna," *IEEE Antennas Wireless Propag. Lett.*, vol. 17, pp. 1324–1328, 2018.

[21] X. Yang, H. Lin, H. Gu, L. Ge, and X. Zeng, "Broadband pattern diversity patch antenna with switchable feeding network," *IEEE Access*, vol. 6, pp. 69612–69619, 2018.

[22] R. Garg, P. Bhartia, I. Bahl, and A. Ittipiboon, *Microstrip Antenna Design Handbook*. Norwood, MA, USA: Artech House, 2001.

[23] Q.-X. Chu, D.-L. Wen, and Y. Luo, "A broadband ±45° dual-polarized antenna with Y-shaped feeding lines," *IEEE Trans. Antennas Propag.*, vol. 63, no. 2, pp. 483–490, Feb. 2015.

[24] C. Cao and C. Guo, "A wideband high-gain LHCP/RHCP patch antenna based on mirror feed method," *IEEE Antennas Wireless Propag. Lett.*, vol. 21, pp. 2317–2321, 2022.

[25] B. Edward and D. Rees, "A broadband printed dipole with integrated balun," *Microw. J.*, vol. 30, no. 5, pp. 339–344, May 1987.

[26] Y. Sung, "Simple slot antenna with circular polarization diversity," *IEEE Antennas Wireless Propag. Lett.*, vol. 21, no. 4, pp. 690–694, Apr. 2022.

[27] R. Garg, I. Bahl, and M. Bozzi, *Microstrip Lines and Slotlines*. Norwood, MA, USA: Artech House, 1996, p. 126.

YOUNGJE SUNG was born in Incheon, South Korea, in 1975. He received the B.S., M.S., and Ph.D. degrees from Korea University, Seoul, South Korea, in 2001, 2002, and 2005, respectively. From 2005 to 2008, he was a Senior Engineer with the Antenna Research and Development Laboratory, Mobile Phone Division, Samsung Electronics, South Korea. In 2008, he joined the Department of Electronic Engineering, Kyonggi University, Suwon-si, South Korea, where he is currently an Associate Professor. His research interests include reconfigurable antennas, cellphone antennas, wideband slot antennas, multifunction devices, compact circular polarized antennas, and compact dual-mode filters. He is serving as a Reviewer for IEEE Transactions on Microwave Theory and Techniques, IEEE Microwave and Wireless Components Letters, IEEE Antennas and Wireless Propagation Letters, *Progress in Electromagnetics Research*, *Electronics Letters*, *Microwaves, Antennas and Propagation*, and *ETRI Journal* of the Electronics and Telecommunications Research Institute, South Korea.